Millimeter-Wave Photonic Techniques: Part I-Photonic Generation of Millimeter-Wave Signals

Jianping Yao[1], Raman Kashyap[2, 4] Xiupu Zhang[3], and Ke Wu[4]

[1] Microwave Photonics Research Laboratory
School of Information Technology and Engineering
University of Ottawa, Ottawa, Canada

[2] Department of Engineering Physics
Ecole Polytechnique de Montreal, Montreal, Canada

[3] Department of Electrical and Computer Engineering
Concordia University, Montreal, Canada

[4] Poly-Grames Research Center, Department of Electrical Engineering
Ecole Polytechnique de Montreal, Montreal, Canada

Abstract- **Broadband, low loss and cost-effective transmission capability of optical fiber links has led to an ever-increasing interest in their use for the generation and distribution of millimeter-wave (mm-wave) signals for broadband wireless access networks and sensor networks. In this paper, some new techniques in photonic generation of mm-wave signals for radio-over-fiber (RoF) network applications are reviewed, which include phase locking of two ultra-quiet lasers, mm-wave source generation using external modulation techniques.**

Index Terms- **millimeter-wave over fiber, optical generation of millimeter-wave signals, broadband wireless access, optical phase lock loop**

I. INTRODUCTION

The growth of information technology demands significant improvements in communication system capacity, bandwidth, security, mobility, and flexibility. Currently deployed communication systems do not offer these features simultaneously. Optical fiber technology can provide tremendous bandwidth, but it does not support user mobility or flexible system reconfiguration. Wireless communication systems using traditional RF or microwave frequencies can provide user mobility, but they do not support high data rates and security. Usually, high-speed wireless networks may have fundamental limitations with respect to the power budget and user mobility. Wireless communication systems using millimeter-wave (mm-wave) frequencies in the frequency bands of 30 and 60 GHz offer the potential for broadband and secure data transmission platforms, and they have already received considerable interests. Until recently, mm-wave technology was extremely expensive but increased commercial investment in applications such as broadband communication systems (such as IEEE 802.16) has advanced the state-of-the-art of mm-wave components while reducing costs such as the development of substrate integrated circuits (SICs) [1]. Additional cost reductions can be expected as these commercial technologies gain a greater foothold in the marketplace.

A microcellular or picocellular system architecture of 2-200 meters in which mm-wave carriers that deliver high bit rate signals via a radio over fiber (RoF) network to remote wireless base stations or vice-versa will be the most attractive economical and universal solution for seamless broadband multimedia

communications [2, 3] and wireless sensor networks [4, 5].

Key to this technology is the generation and distribution of microwave or mm-wave signals in the optical domain. In the past, extensive investigations of optical microwave generation systems have led to a variety of electrical signal generation methods. These methods employ the techniques such as automatic frequency control loop [6], optical injection locking [7], optical phase-locked loop (OPLL) [8, 9], and external modulation [10-15]. The short- and long-term frequency stability of the optically generated mm-wave signals is critical because the resulting signal is generally used either as a RF carrier or a local oscillator signal in system applications. Optical frequency locking, optical injection locking and OPLL have all been used to improve the long-term frequency stability. An OPLL, when used in combination with a narrow linewidth optical source, can generate an mm-wave signal with high short-term frequency stability [16]. The short-term stability is directly related to the spectral purity of the generated signal and it can be characterized with phase noise measurement techniques. In this paper, we will present three new techniques developed recently by the authors in the generation of mm-wave signals in the optical domain.

II. PHASE LOCKING OF TWO ULTRA-QUIET LASERS

A compact, stable laser with an ultra-narrow line-width is of emerging interest in a number of modern applications, including mm-wave generation for RoF applications. For good performance, these lasers should have low phase-noise and excellent long-term stability. Many techniques have been proposed and demonstrated for these applications. For example, injection locking a single frequency semiconductor distributed feedback (DFB) laser with the side-band of a modulated laser [17], using an OPLL with two DFB lasers to maintain the frequency difference [18], or simply generating a data modulated RF signal from a single DFB laser at the radio frequency of interest [19]. Many of

these techniques work out to be suitable for environments which are temperature stable, and the solutions are not applicable to low-cost, maintenance free, or the operation of remote base-stations. For example, the beat-frequency source using two DFB lasers separated in frequency by the RF carrier requires extremely fast feed-back loops of in the range of ns to maintain the long-term stability of the carrier. This inevitably adds to the cost of the system. For other directly RF modulated optical sources, the expense of high frequency bulky components makes them unsuitable for compact, low cost applications. What is needed is a source of high long-term stability with reduced requirements for control loops and components. Additionally, the constraints imposed by the selection of specific DFB wavelengths should also be relaxed.
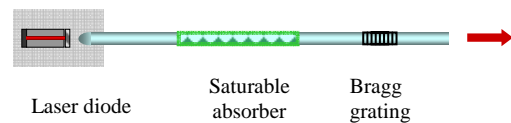

Fig. 1. Semiconductor laser with saturable absorber in the external cavity.

Our recent work has focused on the study of these low cost solutions using a pair of highly stable single frequency sources [20], in which the specification for control loops is considerably relaxed. A linewidth of a few kHz and an exceptional long-term wavelength stability have been demonstrated for a semiconductor laser with an external FBG (FBG) by the presence of a piece of saturable absorber (SA) within the external cavity [21-24], as can be seen in Fig. 1. The doped fiber has a very strong photon absorption, which can be bleached within the whole absorption band by pumping with a narrow line-width source [24]. In a laser with a doped fiber in the external cavity, an effect of broadband bleaching of absorption in the SA and a standing wave, formed in the external cavity by the counter-propagating fields, initiate spatial hole-burning in the SA. The spatial hole-burning and bleaching of absorption induced by high power in the cavity, leads to a dynamic modulation of the absorption, as well as the

refractive index modulation along the length of the SA [24]. This forms a new narrow-bandwidth dynamic grating at the operating wavelength of the laser. Due to this intra-cavity grating within the doped fiber of a long (> 10 cm) external-cavity laser, which otherwise would operate in more than 100 longitudinal modes, it can have a spectrum of a few or even a single longitudinal mode. Spectral line narrowing in a doped fiber external cavity laser (DFECL) has been observed experimentally in lasers at 980 nm, 1480 nm, and 1530 nm with Yb- and Er-doped fiber [21-23].

Using RF spectrum analyzer measurements, we have recently shown that the number of oscillating modes decreases from about 150 in a laser without SA to 5 in a laser with an intra-cavity SA [23]. The measurements, conducted for the DFECL with the laser diode at 1490 nm have also shown a significant reduction in the line-width of the laser and side-mode suppression of the secondary longitudinal modes (adjacent to the dominant mode).

In the DFECL, the SA in the external cavity is pumped at a wavelength of an external FBG mirror (1490 nm or 1530 nm for Er-doped fiber and 976 nm for Yr-doped fiber) and therefore the absorption and emission are at the same wavelength. We refer to this as "inband" pumping. Even though inband-pumping has been used in a few devices [21, 22], there has been no previously reported comprehensive measurement of saturable absorption in such a true two-level system. We have studied this characteristic for the first time in [24] by inband pumping of erbium-doped fiber (EDF) with a narrow-bandwidth laser source and demonstrated a strong broadband bleaching of the absorption.

We have shown that the narrow-linewidth pumping at any single wavelength within the absorption band results in the bleaching of the entire absorption spectrum of the EDF [24]. The depth of the bleaching in the EDF depends on the pump power and the pump wavelength. Fig. 2 shows the absorption bleaching characteristic of CorActive EDF which was measured using the method described in [24]. The EDF was pumped

at 1490 nm by a narrow-linewidth source and the spectra at various pump powers were recorded. The maximum bleaching of absorption was 30 dB/m, measured at the peak of the absorption spectrum at 1528 nm. The absorption is bleached by about 15 dB/m at 1490 nm when the pump power is about 6.7 dBm. Via the Kramers-Kronig relations we have derived the induced changes in the refractive index due to the absorption bleaching at 1490 nm: $\Delta n \sim 1.68 \times 10^{-6}$ (at this pump power for this particular fiber). From the refractive index change one may estimate the coupling constant of a dynamic grating in this doped fiber: $\kappa L \sim 0.3$ (for the length of the doped fiber L = 20 cm). The measured characteristics of the saturable absorption of the EDF provide the key parameters for modeling of the lasers with the SA in the external cavity.
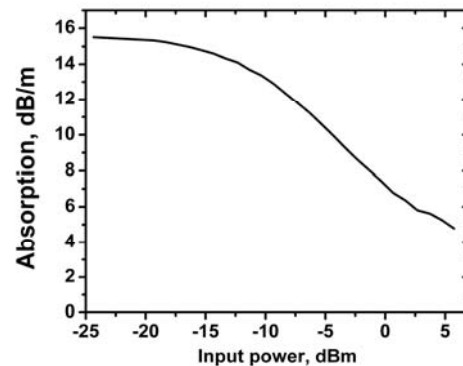

Fig. 2. Absorption of EDF at 1490 nm as a function of pump power at the same wavelength [25].

Recently, we have proposed a new dynamic model of a laser with a SA in the external cavity, which numerically describes the effect of absorption bleaching [20]. We have used our earlier experimental observation of power-dependent absorption bleaching in Er- and Yb-doped fiber (see, for example, Fig. 2). In the DFECL several round-trips of the light in the laser cavity increase the optical power inside the DFECL. This bleaches the absorption gradually according to Fig. 2. The power-dependent absorption bleaching and spatial hole burning, caused by the standing wave in the cavity, result in the absorption modulation along the doped fiber leading to an absorption (loss) grating. In

this grating, the absorption varies between bleached (according to the Fig. 2) and not bleached (α_{max}) absorption. This absorption grating induces a dynamic refractive index grating via the Kramers-Kronig relations. The absorption and the refractive index gratings form a unified "dynamic grating".
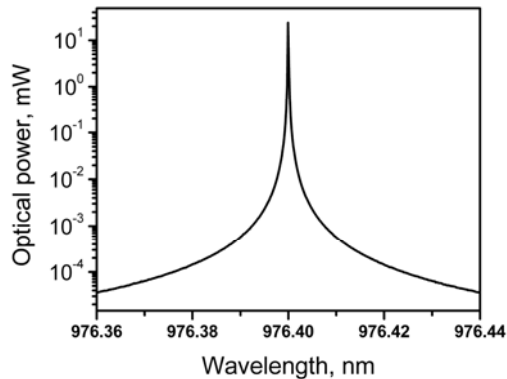

Fig. 3. Simulated spectrum of an optimized DFECL [20].

The absorption and refractive index modulation both contribute to the single-longitudinal-mode generation of the DFECL. Our simulations have shown that the absorption grating is essential for side-mode suppression, though it may lead to the generation of several modes in the spectrum. The single-mode spectrum is possible due to the refractive index grating, which then aids in a faster transition of the spectrum to the single-mode regime. Even though the refractive index grating may not by itself cause side-mode suppression, its contribution is not negligible in the single-mode operation of these lasers.

With this time-domain numerical model we have attempted to confirm the theory of spectral line-narrowing due to the SA, suggested earlier as a result of experimental observations. For the first time to our knowledge, the evolution of the spectrum in a DFECL has been numerically analyzed [20]. In order to demonstrate the potential of our model and the possibility of designing a single-longitudinal-mode (SLM) laser using the algorithm, we have chosen the parameters, which show clearly the evolution of

the dynamic grating and SLM generation. We have shown that after the dynamic grating is established inside the doped fiber, the laser spectrum becomes SLM with ~ 27 dB side-mode suppression ratio as shown in Fig. 3. The laser remains in a SLM regime for the rest of the simulation time, up-to 10 microseconds, which leads to the conclusion that once the laser has reached the SLM regime, it becomes very stable [20].

The stability of the DFECL and the possibility of tuning its wavelength, in order to match accurately the detuning between this wavelength and the wavelength of a second source, used to generate the RoF signal, have also been studied [26]. By changing the parameters such as temperature or drive current of the diode, the laser wavelength may be precisely and continuously tuned within the range of 100 pm. This may allow one to precisely mismatch the wavelengths of two sources for the application in RoF.

On the other hand, the DFECL is a very stable laser with regard to the drive current changes [26, 27]. The wavelength-current characteristic of the DFECL is shown in Fig. 4, at a constant temperature of the diode. At 21°C, the lasing threshold is ~ 30 mA. The wavelength tunes smoothly and continuously over 60 pm (~ 8.1 GHz) when the current is ramped by 160 mA. The linear slope of the change in the laser frequency due to the bias current is approximately 50 MHz/mA (0.375 pm/mA). This is at least 10 times lower than in a conventional external-cavity laser and more than 20 times lower than in a DFB. The current-induced shift of the wavelength in this laser is reduced considerably due to the excess length of the external cavity.

The temporal wavelength stability of the laser has also been measured. At a constant drive current and diode temperature the lasing mode wavelength is stable within the range of ±1 pm for more than 30 minutes [27]. Due to the presence of the long piece of the doped fiber in the cavity and consequently the lifetime of the

dynamic grating, the laser responds slowly to any environmental or mechanical changes and therefore maintains a constant operating wavelength over the lifetime (~10 ms). This phenomenal stability of the DFECL results in its potential advantage for RoF applications: it requires no fast feed-back loop (ns) to maintain the long-term stability of the carrier, which is imperative for the DFB. This quality of the DFECL may significantly reduce the cost of the RoF system. On the other hand, the wavelength may be tuned precisely using a feedback due to the laser tuning characteristics as discussed above.
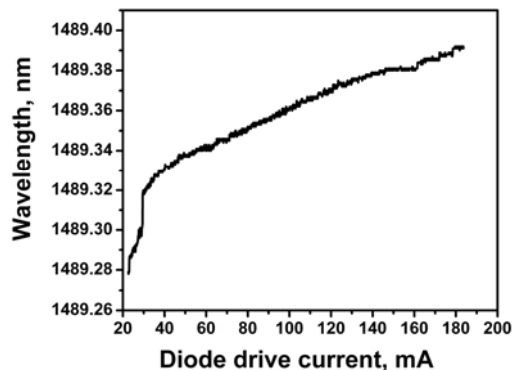
Fig. 4. Static chirp of the DFECL at 21°C [10].

Although self-mode beat may be used to generate stable microwave signals, heterodyne beat-signal generation is preferable for RoF applications as it is tunable and has an extremely wide frequency range, from megahertz to terahertz. We have generated the heterodyne beat signals of two DFECLs by coupling them using a fibre coupler, and measured the output simultaneously with an optical spectrum analyzer and a RF spectrum analyzer (using a photodetector with a bandwidth of 15 GHz). The peak wavelengths of the DFECLs were adjusted to ~1489.8 nm and ~1489.9 nm and therefore the beat signal was measured at ~ 10 GHz by a RF spectrum analyzer.

Fig. 5 shows the heterodyne beat–notes of the two DFECLs [23, 25]. The notes lie mostly within the range of 9 ± 0.5 GHz with the envelope of the Gaussian function. As the DFECLs, used in this particular experiment, had several longitudinal modes in the output, the

heterodyne beat notes in Fig. 5 are the superposition of beating of all frequencies, including heterodyne and self-mode beating. The dominant beat note has a maximum amplitude of -3 dBm and is the heterodyne beat note of the dominant longitudinal modes of two DFECLs. The adjacent notes, which are the superposition of beating of the dominant modes with the side modes, are ~15 dB to 20 dB weaker than the peak note. This indicates that the side modes of each DFECL are suppressed by more than 15 dB. The weaker signals are caused by the beating of the high-order side modes with the dominant modes and the side modes with each other. Since only 10 beat signals are suppressed by less than 50 dB, one may conclude that the DFECLs in this experiment had maximum of 5 oscillating longitudinal modes. Additionally, a narrowband filter may be used to dramatically improve the side-mode suppression.
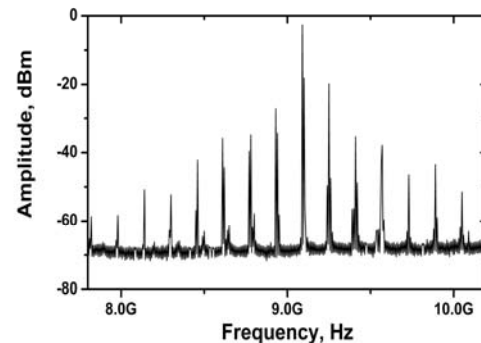

Fig. 5. Measured heterodyne beat-notes from two DFECLs [23].

However, the side modes of the laser may be suppressed significantly by appropriate design of the external cavity: by optimizing the FBG, doped fiber, and the length of the cavity. The external FBG must provide sufficient reflectivity to generate high-power external-cavity mode inside the DFECL and bleach the absorption of the SA. Furthermore, the ratio of the bandwidth of the dynamic grating to the longitudinal mode spacing of the laser defines the maximum number of the oscillating longitudinal modes in the DFECL [23]. According to the simulations, the DFECL with a piece of the SA occupying

most of the external cavity operates at SLM for different drive currents even with slight changes of the fiber length [20].

Our multiple experiments and simulations have shown that the DFECL may be designed as a stable SLM ultra-narrow-linewidth source. Our present work focuses on the improvement of the DFECLs-generated microwave signal by the design and implementation of an optimized SLM DFECL source for RoF communications. We have, however, demonstrated such lasers and their suitability for use in such systems. Further work is in hand to fabricate these potentially low-cost lasers for application in a variety of systems, such as RoF and sensors.

III. MM-WAVE GENERATION USING EXTERNAL MODULATION TECHNIQUES

Being different from the approach using two phase-locked laser diodes to generate a high-quality mm-wave signal, in this Section we present two approaches based on external modulation techniques to generate tunable mm-wave signals with high system stability and low phase noise [28, 29]. For system applications with frequency reconfigurability such as wideband surveillance radar, spread-spectrum or software-defined radio, continuously tunable mm-wave signals are highly desirable. The generation of a wideband, continuously tunable, single-frequency, mm-wave signal using fixed optical filters and narrow bandwidth optical modulators then becomes very attractive.

A. Intensity-Modulator-Based Approach

In the first approach [28], continuously tunable mm-wave signal was generated without using a tunable optical filter. The system consists of an optical intensity modulator which is biased to suppress the odd-order optical sidebands. A FBG serving as a wavelength fixed notch filter is then used to filter out the optical carrier. A stable, low-phase noise mm-wave signal that has 4 times the frequency of the electrical drive signal is generated at the output of a photodetector. A 32 to 50 GHz mm-wave signal is observed on an

electrical spectrum analyzer when the electrical drive signal is tuned from 8 to 12.5 GHz. The quality of the generated mm-wave signal is maintained after transmission over a 25-km standard single mode fiber (SSMF).
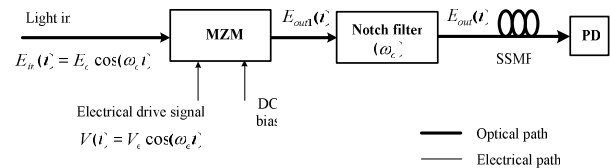

Fig. 6. Diagram of the microwave signal generation system using an IM.
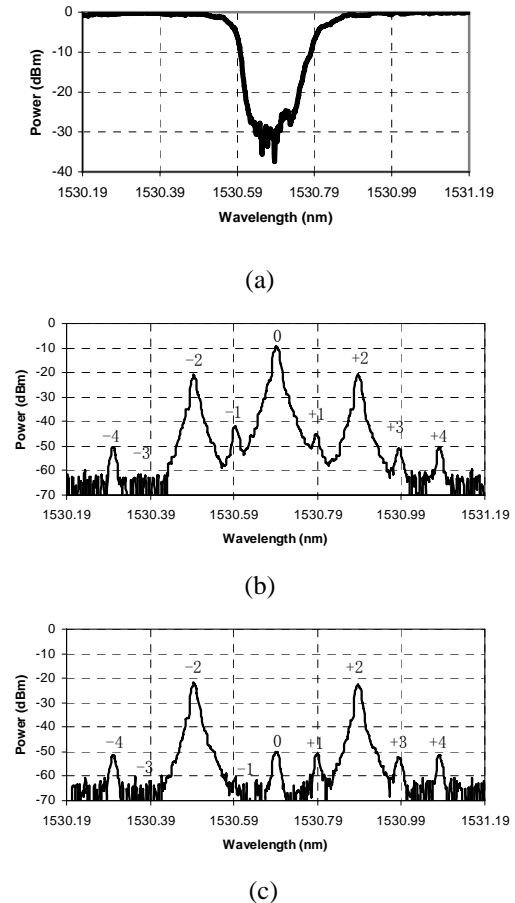

(a)

(b)

(c)

Fig. 7. (a) Transmission spectrum of the FBG filter. (b) Optical spectra before the FBG. (c) After the FBG.

The mm-wave signal generation system using an IM is shown in Fig. 6. An electrical drive signal is applied to the Mach-Zehnder modulator

(MZM), which is biased to suppress the odd-order optical sidebands. An optical notch filter is connected at the output of the MZM to remove the optical carrier. In the experiment, the notch filter is an FBG. The transmission spectrum of the FBG is shown in Fig. 7(a). Fig. 7(b) shows the spectrum after the MZM, with odd-order sidebands suppressed. Two second-order optical sidebands are then obtained at the output of the FBG. A beat note with four times the frequency of the electrical drive signal is generated at a photodetector.
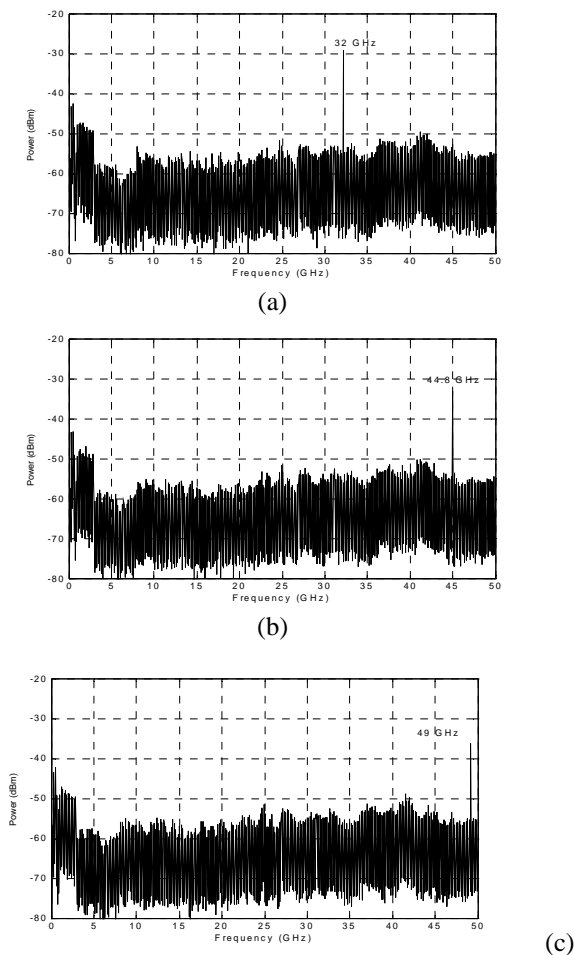

(a)

(b)

(c)

Fig. 8. The spectra of the generated mm-wave signals. (a) 32 GHz. (b) 44.8 GHz. (c) 49 GHz.

Fig. 8 shows the spectra of the generated electrical signals when the microwave drive signal is tuned at 8, 11.2 and 12.25 GHz. Beat

signals with frequencies four times of the drive signals are generated. It can be seen from Fig 8 that mm-wave signals at the frequency of 32, 44.8, and 49 GHz are generated. The spectra are very clean, no other beating signals can be observed across the 50 GHz band. Fig. 9 gives zoom-in views of the beat signal generated locally and remotely after transmission over 25-km signal mode fiber. The frequency of the electrical drive signal is tuned at 12.5 GHz, the generated mm-wave signal is at 50 GHz. As can be seen, the quality of the remotely generated signal is maintained, which demonstrates that the signal is not seriously affected by the chromatic dispersion of the 25-km SSMF.
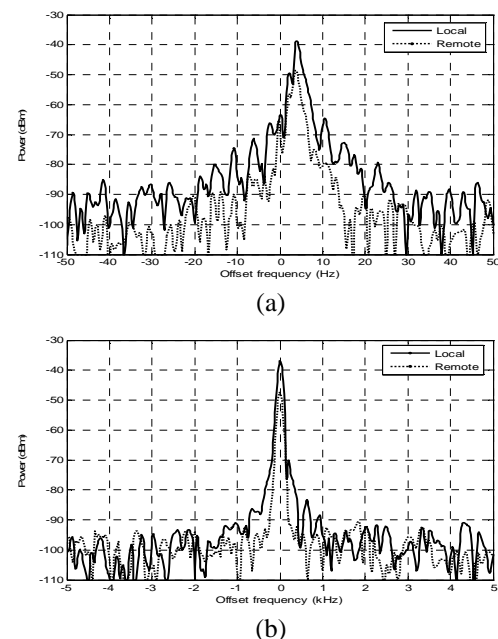

(a)

(b)

Fig. 9. Spectra of the 50-GHz signal generated locally and remotely. (a) Frequency span of 10 kHz. (b) Frequency span of 100 Hz.

The lowest frequency of 32 GHz that can be generated by the proposed system is determined by the bandwidth of the FBG notch filter. With a narrower optical notch filter, this frequency could be much lower than 32 GHz. On the other hand, the highest frequency of the generated signal is only limited by the bandwidth of the optical IM. The IM used in the experiment can operate up to

15 GHz, so the highest frequency of the generated mm-wave signal can reach up to 60 GHz. Due to the bandwidth limitation of the photodetector and the electrical spectrum analyzer, the 60 GHz signal was not observed in electrical domain. However, optical spectrum observation supports the 60 GHz signal generation.

B. Phase-Modulator-Based Approach

The approach using an intensity modulator to generate mm-wave signal, as discussed above, can produce a high-quality frequency-tunable mm-wave signal with a simple system structure. However, to suppress the odd- or even-order optical sidebands, the IM should be biased in the nonlinear region, which would cause the bias-drifting problem, leading to poor system robustness. A solution to this problem is to use an optical phase modulator (PM) since no bias adjustment is required [29]. An experimental setup used to generate mm-wave using an optical PM is illustrated in Fig. 10.
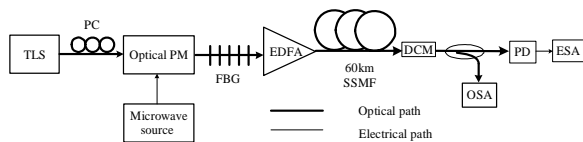

Fig. 10. Experimental setup for optical generation of mm-wave signals using a PM.

The optical carrier generated by a tunable laser source (TLS) is sent to the PM through a polarization controller (PC). The wavelength of the optical carrier is set to match the maximum attenuation wavelength of the FBG. A microwave signal source tunable from 12.5 to 25 GHz is applied to the PM. Optical sidebands at the output of the FBG are amplified with an erbium-doped fiber amplifier (EDFA), and then transmitted over 60 km of SSMF. The beat of these optical sidebands at a photodetector generates the required mm-wave signals. The transmission spectrum of the FBG notch filter is the same as the one shown in Fig. 7(a). The bandwidth from the minimum attenuation point

at lower wavelengths to the minimum attenuation point at longer wavelengths is about 0.3 nm ($\approx$ 37.5 GHz).
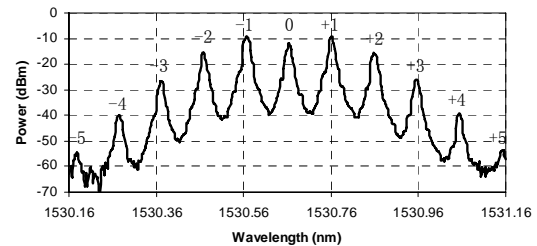
(a)
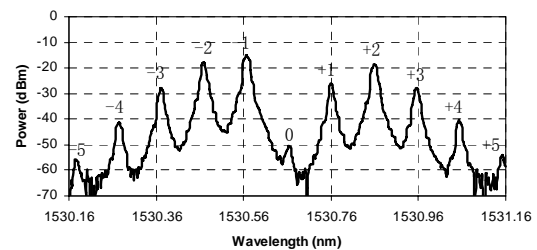
(b)

Fig. 11. Typical optical spectra before transmission. (a) Before the FBG filter. (b) After the FBG filter.

As can be seen in Fig. 7(a), the attenuation of the FBG filter on its lower and upper frequency slopes is not symmetrical with respect to the center of the notch. As such the group delay is also not symmetrical. If the sidebands of the modulated optical signal fall in this section of the filter bandwidth, the non-symmetrical characteristic will destroy the intrinsic amplitude and phase relationship among the optical sidebands of a phase modulated signal. The power of the required mm-wave signal and the odd-order harmonic suppression will be affected. To avoid this, the electrical drive signal must have a low frequency criterion. The lowest frequency of the electrical drive signal should be equal to or greater than half of the frequency bandwidth of the FBG. In this case, the generated mm-wave signal is only affected by the maximum attenuation at the center of the notch, and it is immunized from the imperfect characteristics of the FBG including its large dispersion effect.
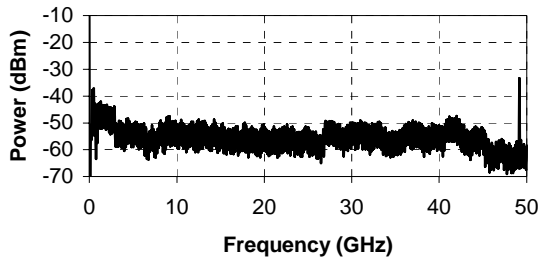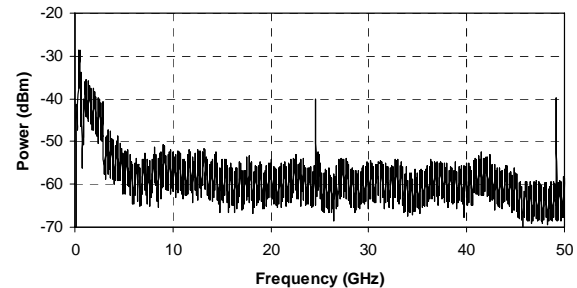
Fig. 12. Spectrum of the generated mm-wave signal when the drive signal frequency is 24.5 GHz.

Measurements were taken before and after transmission, with and without dispersion compensation in order to analyze and evaluate the performance of the system. Fig. 11 shows the typical optical spectra before and after the FBG filter. Here the optical PM is driven by a 12.5-GHz signal. Fig. 11(a) shows that optical sidebands are generated up to the fourth order. They are distributed symmetrically around the optical carrier. Fig. 11(b) shows the optical spectrum after the FBG filter. It is clearly shown that the optical carrier power is attenuated about 40 dB. Due to the bandwidth of the FBG and its asymmetric attenuation characteristics, the first-order optical sidebands are not attenuated to the same level on the two sides of the carrier. This is an issue for drive frequencies up to about 19 GHz for this particular FBG, but the problem can be avoided by operating at higher frequencies or by improving the spectrum symmetry of the FBG.

Fig. 12 shows the spectrum of the optically generated electrical signal, measured at the output of the photodetector before transmission. The spectrum corresponds to a 24.5 GHz electrical drive signal – a frequency where the first-order optical harmonics are not attenuated by the FBG. It is easily seen that an mm-wave signal at twice the frequency of the drive electrical signal is generated. Signal components above 50 GHz are not visible due to the bandwidth limit of the photodetector and the electrical spectrum analyzer; however, they are present in the output when viewed on the optical spectrum analyzer. When the electrical drive signal is tuned from 18.8 to 25 GHz, two bands

of mm-wave signals from 37.6 to 50 GHz and from 75.2 to 100 GHz with high frequency stability and narrow linewidth are generated.

(a)
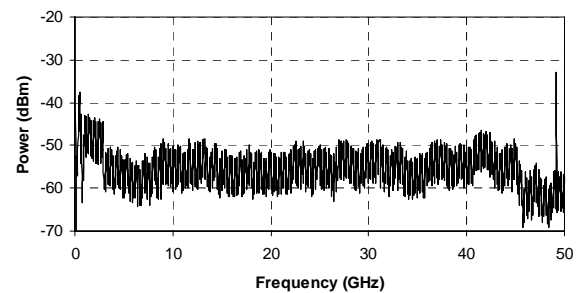
(b)

Fig. 13. Spectra of the generated mm-wave signals after transmission over 60 km SSMF. (a) Without and (b) with dispersion compensation.

Fig. 13 shows the electrical spectra of the remotely generated electrical signals when the electrical drive signal is at 24.5 GHz, after propagation over 60 km SSMF. Fig. 13(a) is an indication of the spectrum without dispersion compensation while Fig. 13(b) is the spectrum when dispersion compensation is applied before photodetection. In Fig. 13(a), the 24.5-GHz signal is not fully cancelled and the amplitude of the 49-GHz signal decreases due to a chromatic-dispersion-induced power penalty. Fig. 13(b) clearly shows the cancellation of the 24.5-GHz signal and the elimination of the power penalty to the 49-GHz signal when chromatic dispersion compensation is used.

Fig. 14 gives zoom-in views of the electrical spectra of the optically generated 49-GHz electrical signal before and after transmission with dispersion compensation. The resolution

bandwidth of the electrical spectrum analyzer is 1 Hz and 100 Hz in Fig. 14(a) and Fig. 14(b), respectively. It can be seen that the 49-GHz electrical signal does not suffer from obvious phase noise degradation after the 60-km transmission. The quality of the signal is adequate for most practical applications.
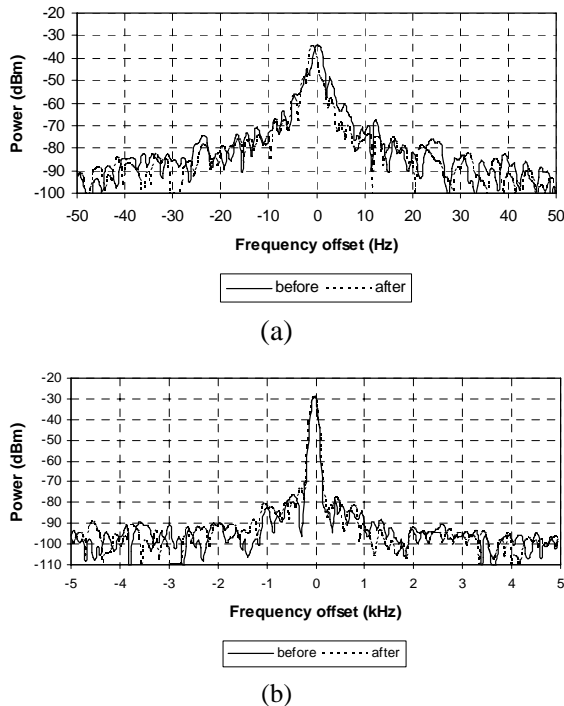

(a)

(b)

Fig. 14. Electrical spectra of the signal generated before and after transmission with dispersion compensation (a) Span of 100 Hz. (b) Span of 10 kHz.

IV. CONCLUSION

Photonic techniques provide many advantages over electronic counterpart for the generation of wideband, tunable mm-wave signals for applications such as broadband wireless access networks and sensor networks. In this paper, three new approaches developed recently by the authors to generate mm-wave signals have been presented. These approaches are suitable for RoF applications. The key challenge in implementing these techniques in RoF networks is the large size and high cost of the optical components and devices. The use of the innovative SIC technology would be a solution to this problem.

REFERENCES

[1]   D. Deslandes and K. Wu, "Single-substrate integration technique of planar circuits and waveguide components," *IEEE Trans. Microwave Theory Tech.,* vol. 51, pp. 593-596, Feb. 2003.

[2]   W. D. Jemison, P. R. Herczfeld, W. Rosen, A. Vieira, A. Rosen, A. Paolella, and A. Joshi, "Hybrid fiber-optic millimeter-wave links," *IEEE Microwave Mag.*, vol. 1, pp. 44-51, Jun. 2000.

[3]   E. I. Ackerman, C. H. Cox, "RF fiber-optic link performance," *IEEE Microwave Mag.,* vol. 2, pp. 50-58, Dec. 2001.

[4]   C. Y. Chong and S. P Kumar, "Sensor networks: evolution, opportunities, and challenges," Proc. of the IEEE , vol. 91, no. 8, pp.1247-1256, Aug. 2003.

[5]   D. R. Martinez and M. Gruber, "Next generation technologies to enable sensor networks," *Proc. of IEEE Sensors,* vol. 2, pp. 1468-1472, Jun. 2002.

[6]   R. P. Braun, G. Grosskopf, D. Rohde, and F. Schmidt, "Optical millimetre-wave generation and transmission experiments for mobile 60 GHz band communications," *Electron. Lett.*, vol. 32, pp. 626-628, 1996.

[7]   L. Goldberg, H. F. Taylor, J. F. Weller, and D. M. Bloom, "Microwave signal generation with injection-locked laser diodes," *Electron. Lett.*, vol. 19, pp. 491-493, 1983.

[8]   R. T. Ramos and A. J. Seeds, "Fast heterodyne optical phase lock loop using double quantum well laser diodes," *Electron. Lett.*, vol. 28, pp. 82-83, 1992.

[9]   L. N. Langley, M. D. Elkin, C. Edge, M. J. Wale, U. Gliese, X. Huang, and A. J. Seeds, "Packaged semiconductor laser optical phase-locked loop (OPLL) for photonic generation, processing and transmission of microwave signals," *IEEE Trans. Microwave Theory Tech.*, vol. 47, pp. 1257-1264, Jul. 1999.

[10]   J. J. O'Reilly, P. M. Lane, R. Heidemann, and R. Hofstetter, "Optical generation of very narrow linewidth millimetre wave signals," *Electron. Lett.*, vol. 28, pp. 2309-2311, 1992.

[11] J. J. O'Reilly and P.M. Lane, "Fibre-supported optical generation and delivery of 60 GHz signals," *Electron. Lett.*, vol. 30, pp. 1329–1330, 1994.

[12] P. Shen, N. J. Gomes, P. A. Davies, W. P. Shillue, P.G. Huggard, and B. N. Ellison, "High-purity millimetre-wave photonic local oscillator generation and delivery," in *Proc. Microwave Photonics,* pp. 189-192, 2003.

[13] P. O. Hedekvist, B. E. Olsson, and A. Wiberg, "Harmonic generation of photonic microwave frequencies utilizing the properties of a phase modulator," in *Proc. Microwave Photonics,* pp. 193-196, 2003.

[14] X. J. Meng and J. Menders, "Optical generation of microwave signals using SSB-based frequency-doubling scheme," *Electron. Lett.*, vol. 39, pp. 103-105, 2003.

[15] G. Qi, J. P. Yao, J. Seregelyi, S. Paquet, and J. C. Bélisle, "Millimeter-wave carrier generation using an optical phase modulator and an optical notch filter," in *Proc. Photonics North 2004,* vol. SPIE-5579C, paper 102.

[16] F. N. Timofeev, S. Bennett, R. Griffin, P. BayveL, A. J. Seeds, R. Wyatt, R. Kashyap, and M. Robertson, "High spectral purity millimetre-wave modulated optical signal generation using fibre grating lasers," *Electron. Lett.*, vol. 34, pp. 668-669, 1998.

[17] R. P. Braun, G. Grosskopf, D. Rohde, and F. Schmidt, "Low-phase-noise millimeter-wave generation at 64 GHz and data transmission using optical sideband injection locking," *IEEE Photon. Technol. Lett.*, vol. 10, pp.728-730, May 1998.

[18] U. Gliese, T. N. Nielsen, S. Norskov, and K. E. Stubkjaer, "Multifunctional fiber-optic microwave links based on remote heterodyne detection," *IEEE Trans. Microwave Theory Tech.*, vol. 46, pp. 458-468, May 1998.

[19] K. E. Razavi and P. A. Davies. "Millimetre wave generation by filtering the FM-IM spectra of a directly modulated DFB laser," *IEEE MTT-S International Microwave Symposium Digest*, vol.3, pp. 1707-1708, Jun. 1997.

[20] I. A. Kostko and R. Kashyap, "Dynamics of ultimate spectral narrowing in a semiconductor fiber-grating laser with an intra-cavity saturable absorber," *Opt. Express*, vol. 14, pp. 2706-2714, Apr. 2006.

[21] W. H. Loh, R.I. Laming, M. N. Zervas, M. C Farries, and U. Koren, "Single frequency erbium fiber external cavity semiconductor laser," *Appl. Phys. Lett.*, vol. 66, pp. 3422-3424, 1995.

[22] F. N. Timofeev and R. Kashyap, "High-power, ultra-stable, single-frequency operation of a long, doped-fiber external-cavity, grating-semiconductor laser," *Opt. Express*, vol. 11, pp. 515-520, Mar. 2003.

[23] R. Liu, I. Kostko, K. Wu, and R. Kashyap, "Optical generation of microwave signal by doped fiber external cavity semiconductor laser for radio-over-fiber transmission," *Proc. SPIE, Photonic Applications in Nonlinear Optics, Nanophotonics, and Microwave Photonics*, R. A. Morandotti, H. E. Ruda, J. P. Yao, Eds., vol. 5971, pp. 455-462, Sep. 2005.

[24] R. N. Liu, I. A. Kostko, R. Kashyap, K. Wu, and P. Kiiveri, "Inband-pumped, broadband bleaching of absorption and refractive index changes in erbium doped fiber," *Opt. Commun.* vol. 255, pp. 65-71, Nov. 2005.

[25] R. Liu, I. A. Kostko, K. Wu, and R. Kashyap, "Side mode suppression by doped fiber in long external cavity semiconductor laser operating at 1490 nm," *prepared for publication.*

[26] R. Liu, I. Kostko, K. Wu, and R. Kashyap, "Tuning characteristics of erbium doped fiber long external cavity semiconductor laser for radio-over fibre applications," *Proc. SPIE, Photonics North*, Quebec, Canada, June 2006.

[27] R. Liu, I. Kostko, K. Wu, R. Kashyap. *Manuscript in preparation for publication.*

[28] G. Qi, J. P. Yao, J. Seregelyi, C. Bélisle, and S. Paquet, "Generation and distribution of a wideband continuously tunable mm-wave signal with an optical external modulation technique," *IEEE Trans. Microwave Theory Tech.,* vol. 53, no.10, pp. 3090-3097, Oct. 2005.

[29] G. Qi, J. P. Yao, J. Seregelyi, C. Bélisle, and S. Paquet, "Optical generation and distribution of continuously tunable millimeter-wave signals using an optical phase modulator," *J. Lightwave Tech.*, vol. 23, no.9, pp. 2687-2695, Sep. 2005.